Correlation between structure and magnetic anisotropies of Co on Cu(110)

J. Fassbender* and G. Güntherodt
2. Physikalisches Institut, Rheinisch-Westfälische Technische Hochschule Aachen, D-52056 Aachen, Germany

C. Mathieu and B. Hillebrands
Fachbereich Physik, Universität Kaiserslautern, D-67663 Kaiserslautern, Germany

R. Jungblut, J. Kohlhepp,† and M. T. Johnson
Philips Research Laboratories, NL-5656 AA Eindhoven, The Netherlands

D. J. Roberts and G. A. Gehring
Department of Physics, University of Sheffield, Sheffield S3 7RH, United Kingdom
(Received 8 October 1997)

Magnetic anisotropies of molecular-beam-epitaxy-grown fcc Co(110) films on Cu(110) single-crystal substrates have been determined by using Brillouin light scattering and have been correlated with the structural properties determined by low-energy electron diffraction and scanning tunneling microscopy (STM). Three regimes of film growth and associated anisotropy behavior are identified: coherent growth in the Co film thickness regime of up to 13 Å, in-plane anisotropic strain relaxation between 13 and about 50 Å and in-plane isotropic strain relaxation above 50 Å. The structural origin of the transition between anisotropic and isotropic strain relaxation was studied using STM. In the regime of anisotropic strain relaxation long Co stripes with a preferential $[1\bar{1}0]$-orientation are observed, which in the isotropic strain relaxation regime are interrupted in the perpendicular in-plane direction to form isotropic islands. In the Co film thickness regime below 50 Å an unexpected suppression of the magnetocrystalline anisotropy contribution is observed. Symmetry reflections based on a crystal-field formalism and discussed within the context of band theory, which explicitly takes tetragonal misfit strains into account, reproduce the experimentally observed anomalies despite the fact that the thick Co films are quite rough. [S0163-1829(98)03810-7]

I. INTRODUCTION

Magnetic anisotropies in a thin ferromagnetic film are significantly modified compared to those in the respective bulk material. This is due to changes of the structural symmetry in the film caused by misfit strains as well as due to the occurrence of surface anisotropy contributions. The large fraction of atoms located at surface or interface sites are in a reduced-symmetry atomic environment generating lower-order anisotropy contributions of the Néel type[1] at each of these sites. It is therefore not surprising that large interface anisotropies are found, which exceed the magnetocrystalline bulk anisotropy, which is the leading anisotropy contribution existing in an infinite $3d$ transition-metal medium, by several orders of magnitude. In performing the transition from a bulk medium to a thin film, it is therefore of great interest to follow the magnetocrystalline anisotropy and to investigate its transition into thin-film anisotropies. Presumably due to its weak contribution in thin films in the presence of large lower-order film anisotropies the magnetocrystalline bulk anisotropy has not been investigated so far in this regime.[2]

The aim of this paper is to investigate the thickness dependence of all contributing magnetic anisotropies in fcc(110)-oriented epitaxial Co films with respect to their origin and symmetry. A clear evolution of the strain dependence of all magnetic anisotropy contributions is found in the regimes of pseudomorphic growth and lattice relaxation due to dislocation formation. The development of magnetic bulk anisotropies is highlighted by the sudden onset of the magnetocrystalline anisotropy to its full bulk value near a Co film thickness of 50 Å. All salient properties of the thickness dependence of the magnetic anisotropies are discussed within symmetry reflections based on the crystal-field formalism which explicitly takes tetragonal misfit strains into account. With decreasing film thickness we obtain a transformation of cubic anisotropy into in-plane and out-of-plane uniaxial contributions with increasing uniaxial distortion of the unit cell caused by increasing misfit strain.

Magnetic anisotropies in epitaxial fcc Co films have previously been studied for the (001), (1 1 13), and (111) orientations.[2–15] Although for Co(001) films all contributing anisotropies were quantitatively determined, an identification in terms of magnetoelastic or magnetocrystalline contributions could not be performed due to the higher-order nature of the observed anisotropies.[8] For Co (1 1 13) films the uniaxial in-plane anisotropy was identified as being of magnetoelastic origin due to the elastic strain fields caused by the substrate-film lattice mismatch.[13] The observed perpendicular anisotropy contributions could not be further identified both in the Co(001) and the Co(1 1 13) systems. In particular, in both systems no identification of any magnetocrystalline bulk anisotropy contribution could be made.

To separate the magnetoelastic, the magnetocrystalline, and the Néel-type interface anisotropy contributions a con-

figuration must be chosen, in which these anisotropy contributions appear with characteristically different symmetries and film thickness dependences. This is best achieved in the case of the (110) orientation. In this case the magnetoelastic anisotropy and the Néel-type anisotropy are of twofold symmetry whereas the magnetocrystalline anisotropy has both twofold and fourfold symmetry contributions [(001)-fourfold symmetry rotated into the (110) reference frame]. The easy axes of the magnetocrystalline anisotropy are the ⟨111⟩ axes,[3,4,17] four of which are contained in the (110) surface. A symmetry analysis of the free-energy density permits a separation of all these anisotropy contributions. In addition, Néel interface and magnetoelastic anisotropies can be separated as follows: Néel-type anisotropy contributions, converted into bulk anisotropy contributions[16] show a characteristic dependence on the inverse film thickness, independent of the growth mode of the film. Chappert and Bruno[18] have proposed that lattice misfit strains may contribute via magnetoelastic interaction to the volume anisotropy in coherent structures, i.e., in the pseudomorphic growth regime, and to the thickness-dependent anisotropy terms in incoherent structures, since for the latter the strain relaxation is thickness dependent. From a combined study of coherent and incoherent growth regimes the respective magnetoelastic and Néel-type anisotropy contributions can be separated.

For symmetry reasons both the lowest-order in-plane interface and the magnetoelastic anisotropy contribution have either the [001] or the $[1\bar{1}0]$ axis as the symmetry axis in the film plane. On the other hand, for thick fcc Co films the ⟨111⟩ axes are the easy axes of the magnetocrystalline anisotropy.[3,4,17] All these axes are contained in the (110) surface. Therefore an analysis of the spin-wave frequency measured as a function of the in-plane direction of the external field yields information about all relevant anisotropies. It should be noted here that it has been shown that (110)-oriented Co layers in the fcc structure (instead of hcp) can be grown with thicknesses exceeding 1000 Å.[20]

To separate the different magnetic anisotropy contributions in terms of magnetoelastic, magnetocrystalline, and Néel-type anisotropy contributions it is essential to know as much as possible about the structural properties of the thin Co films and how they change their morphology with increasing thickness. This knowledge leads to a correlation between magnetic anisotropy behavior and the growth of the film, i.e., pseudomorphism and strain relaxation due to dislocation formation. Therefore detailed studies of scanning tunneling microscopy (STM) and low-energy electron diffraction (LEED) have been used to check the film morphology and structure, respectively. The aim of this paper is to show the evolution of the structural properties with increasing film thickness and the resulting magnetic anisotropy behavior.

II. EXPERIMENTAL

The samples used in the present study were molecular-beam-epitaxy-grown in ultrahigh vacuum at a base pressure lower than 10^{-10} mbar with deposition rates of 0.3 Å/s for Co and 0.2 Å/s for Cu, controlled by quartz crystal thickness monitors. The error in determining the absolute layer thicknesses is estimated to be less than 5%. The Cu(110) single-crystal substrates were prepared by Ar^+ sputtering and annealing cycles. Auger electron spectroscopy was used to check the cleanliness of the substrates and the films. The Co layers were prepared by withdrawing an eclipsing shutter during deposition, thus creating a wedge-shaped layer with a well-defined slope for the thin-film thickness range 0–40 Å. For larger film thicknesses of up to 150 Å staircase-shaped layers (Fig. 1) were prepared. In this way the same growth conditions are achieved in a wide range of film thicknesses for the samples.

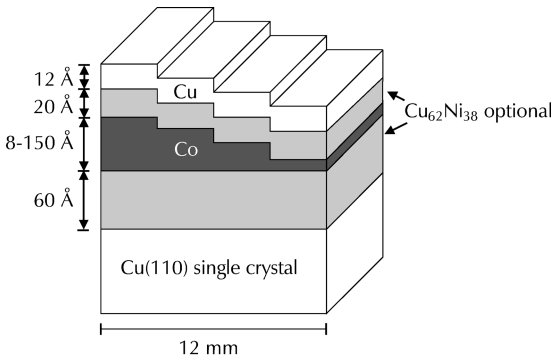

FIG. 1. Schematic sketch of the samples. To test the strain dependence one series of samples is prepared with $Cu_{62}Ni_{38}$ buffer layers reducing the lattice mismatch from -2% to -1%.

Structural studies of the substrate and of the films of different thicknesses were performed by low-energy electron diffraction (LEED) and scanning tunneling microscopy (STM). From LEED-I(V) measurements a tetragonally distorted fcc crystal structure is inferred for the investigated thickness regime. To obtain symmetrical Co/Cu interfaces the Co layers were covered with a 12 Å thick Cu cover layer. Finally, a 25 Å thick protective Au layer was deposited (not shown in Fig. 1). To study the dependence of the anisotropies on the misfit induced strain a series of samples was prepared with $Cu_{62}Ni_{38}$ buffer layers (see Fig. 1) to reduce the lattice mismatch from -2% to -1% and therefore the in-plane strain in the films.

Brillouin light-scattering measurements were performed in backscattering geometry at room temperature using a computer controlled (3+3)-pass tandem Fabry-Perot interferometer with spectral ranges chosen between 30 and 100 GHz as described elsewhere.[21] The incident laser light (514.5 nm Ar^+-line) was focused onto the sample with an angle of incidence of 45° and a power of 100–200 mW. An external field of 0.5–10 kOe was applied parallel to the film plane and perpendicular to the scattering plane. In order to suppress signals from surface phonons the backscattered light was detected by a photomultiplier in the depolarized configuration.

To determine the anisotropy constants we consider a film coordinate system oriented such that the $\hat{x}_1$ and $\hat{x}_2$ axes are parallel to the film plane along the [001] and $[1\bar{1}0]$ direction with the $\hat{x}_3$ axis normal to the film plane; $\hat{x}_{1'}$, $\hat{x}_{2'}$ and $\hat{x}_{3'}$ are the unit vectors in the corresponding coordinate system oriented along the principal crystallographic axes. We describe the properties of the magnetic anisotropies by (i) assuming cubic symmetry of the film, represented by a cubic magnetocrystalline anisotropy constant of fourth order, K_1, (ii) describing the misfit induced tetragonal distortions from

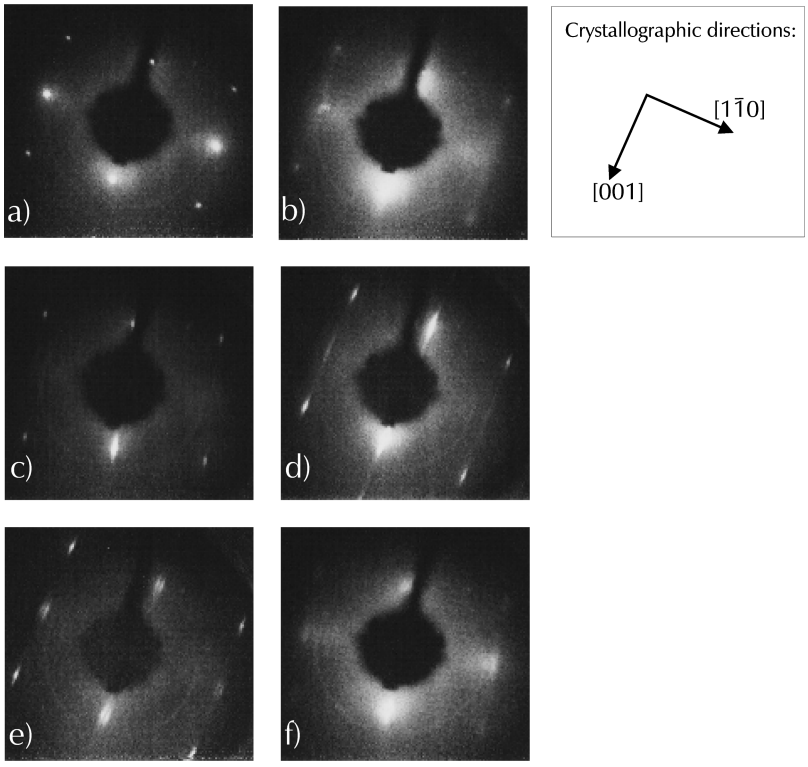

FIG. 2. LEED pattern of (a) a Cu(110) single crystal and (b) for a deposited Co layer of 3–4 Å, (c) 20 Å, (d,e) 30 Å, and (f) 130 Å. The electron beam energy was chosen to be 148 eV except in (e) (110 eV).

cubic symmetry by two additional uniaxial anisotropy contributions of second order $K_{\text{in-plane}}$ and $K_{\text{out-of-plane}}$, which are further composed of thickness-independent and -dependent terms, $K_{\text{in-plane}} = -K_p + (2/d)\,k_p$ and $K_{\text{out-of-plane}} = K_s + (2/d)\,k_s$, with d the film thickness. The magnetoelastic anisotropy depends on $K_{\text{in-plane}}$ and $K_{\text{out-of-plane}}$, whereas Néel-type anisotropies only enter k_s. With $\vec{\alpha}$ the direction unit vector of the magnetization with components α_x, α_y, and α_z expressed in the film coordinate system or $\alpha_{x'}$, $\alpha_{y'}$, and $\alpha_{z'}$ expressed in the crystallographic reference frame, the free anisotropy energy is then expressed as

$$F_{\text{ani}} = K_1(\alpha_{x'}^2\alpha_{y'}^2 + \alpha_{y'}^2\alpha_{z'}^2 + \alpha_{z'}^2\alpha_{x'}^2) + K_{\text{in-plane}}\alpha_x^2 - K_{\text{out-of-plane}}\alpha_z^2. \quad (1)$$

It is observed that the shape anisotropy causes the magnetization to lie in the film plane for the investigated Co thickness range (8–150 Å). Therefore we can set $\alpha_z = 0$ to establish the static in-plane equilibrium direction.

We determined all anisotropy constants contained in Eq. (1) by use of Brillouin light scattering from thermally excited dipolar spin waves propagating along the film plane (Damon-Eshbach modes).[5,8,10,13,23] Due to the precession of the magnetic moments, forming the spin wave, the torques acting on the magnetization, i.e., the two anisotropy field components perpendicular to the mean direction of magnetization, are probed. The spin-wave frequencies are further sensitive to the magnitudes and directions of the magnetization and of the spin-wave wave vector as well as to the film thickness. Explicitly

$$\left(\frac{\omega}{\gamma}\right)^2 = \left(\frac{1}{M_s}\frac{\partial^2 F_{\text{ani}}}{\partial\theta^2} + H\cos(\varphi-\varphi_H) + \frac{2A}{M_s}q^2 + 4\pi M_s f \times\left(1-\frac{1}{2}q_{||}d\right)\right)\left(\frac{1}{M_s}\frac{\partial^2 F_{\text{ani}}}{\partial\varphi^2} + H\cos(\varphi-\varphi_H) + \frac{2A}{M_s}q^2 + 2\pi M_s f q_{||} d\sin^2(\varphi-\varphi_q)\right), \quad (2)$$

with spin-wave frequency ω, gyromagnetic ratio γ, saturation magnetization M_s, applied magnetic field H, exchange constant A, spin-wave vector $q=(q_{||},q_\perp)$, demagnetizing factor f, film thickness d, and angles φ, φ_H, φ_q and θ as in Fig. 5(a). Details of the underlying theory, which is used in a least-squares fit of the measured spin-wave frequencies with the anisotropy constants as free parameters, are described elsewhere.[5,23,24]

III. STRUCTURE

We now discuss the structural properties of the fcc Co(110) films relevant for the interpretation of the magnetic anisotropies in the next section. Figure 2(a) shows a LEED pattern of a well prepared Cu(110) single crystal at an electron beam energy of 148 eV. The sharpness and brightness of the LEED reflections indicate a well ordered and smooth surface. After deposition of 3–4 Å Co [Fig. 2(b)] the LEED pattern has changed greatly. The reflections are very broad and diffuse. This is indicative of the formation of islands at this nominal thickness of 2 monolayers (ML). Figure 3(a) shows the corresponding STM image of a 3 Å thick Co film

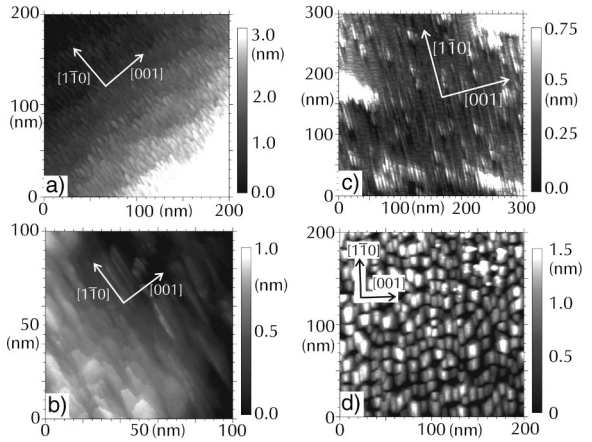

FIG. 3. STM images for a deposited Co film thickness of (a) 3 Å, (b) 20 Å, (c) 30 Å, and (d) 130 Å on a Cu(110) single-crystal substrate.

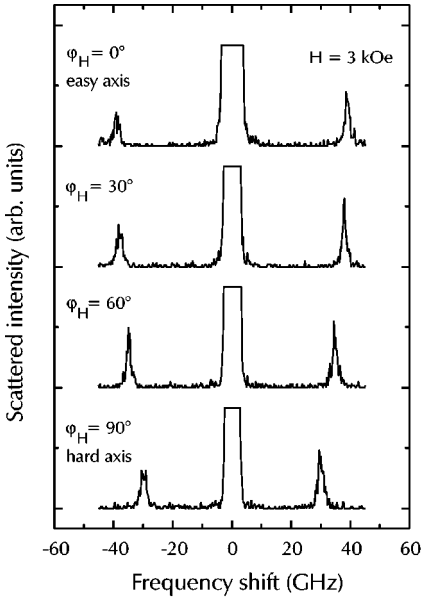

FIG. 4. Spin-wave spectra for a 20 Å thick Co film as a function of the in-plane angle φ_H between the direction of the applied magnetic field of 3 kOe and the [001] direction [see sketch in Fig. 5(a)]. The experimental parameters are laser power=200 mW, free spectral range (FSR)=60 GHz, 200 channels per FSR, dwell time per channel and scan=1 ms, 2000 scans per spectrum.

on a Cu(110) single crystal. Monoatomic steps of the Cu(110) single crystal along the [001] direction are clearly seen. The deposited Co atoms diffuse to the step edges and create 2–3 ML high stripe-shaped islands oriented parallel to the [1$\bar{1}$0] direction. The broad LEED reflections in Fig. 2(b) are due to the large surface roughness in this thickness regime. With further deposition of up to 20 Å Co [Fig. 2(c)] the LEED reflections resharpen, but we observe a streaking of the LEED reflections along the [001] direction. This result indicates that the lattice periodicity along the [1$\bar{1}$0] direction (small width of the reflections) is the same as in the substrate, but along the [001] direction (large width of the reflections) an additional structural order with a broad distribution (no well defined periodicity) takes place due to island formation. These LEED patterns can be explained in terms of an anisotropic surface diffusion of the deposited atoms resulting in anisotropic island shapes. This hypothesis is corroborated by the STM image of a 20 Å thick Co film [Fig. 3(b)]. Strongly stripe-shaped islands with a uniform height are observed. Parallel to the stripe shaped islands (parallel to the [1$\bar{1}$0] direction) the lattice periodicities of the Co film and the Cu substrate are the same, but perpendicular to the stripe shaped islands (parallel to the [001] direction) an additional periodicity arises due to the regular island separations resulting in a broadening of the LEED reflections along this direction. On further increasing the Co film thickness to 30 Å [Fig. 2(d)] we find a broadening of the LEED reflections along the [1$\bar{1}$0] direction as well. This means that an additional distribution of islands occurs in that crystallographic direction. Changing the primary electron energy to 110 eV [(Fig. 2(e)] we observe a distinct splitting of the LEED spots along [1$\bar{1}$0]. The Co films exhibit an additional, induced periodic island arrangement of narrow periodicity distribution along the [1$\bar{1}$0] direction. In the STM image for a 30 Å thick Co film [Fig. 3(c)] we find in addition to the stripe-shaped islands a regular monoatomic step array with the step edges parallel to the [001] direction. Since the terrace widths in this direction are very regular we find a splitting of the corresponding LEED reflections in Fig. 2(e). With further increasing the Co film thickness to 130 Å [Fig. 2(f)] we obtain very broad but nearly isotropic LEED reflections. The layer is now rough, but nearly isotropic in-plane which is also well reproduced by the STM images [Fig. 3(d)]. The surface roughness is very large with an exposed surface of about 10 ML. The island shape in this thickness regime is squarelike. Therefore we expect a nearly fourfold symmetrical behavior of the corresponding shape- and magnetoelastic anisotropy contributions.

The epitaxial growth of the Co/Cu(110) system is qualitatively not as well defined as compared to the Co/Cu(001) system,[25,26] but better than for the (111) orientation.[27–29] In conclusion a small regime of pseudomorphic growth for Co film thicknesses below 14 Å is followed by an intermediate thickness regime dominated by strongly striped island shapes resulting in an anisotropically relaxed strain within the film plane, which is further followed by a gradual transition near 50 Å into a pure island growth and square-shaped islands with in-plane isotropic strain.

IV. MAGNETIC ANISOTROPIES

To investigate the different anisotropy contributions of the fcc Co(110) films we have performed Brillouin light-scattering (BLS) measurements. The spin-wave frequencies are measured as a function of the crystallographic in-plane direction in an applied field of 3 kOe, which is high enough to saturate the magnetization in the hard in-plane magnetization direction. The anisotropy constants are determined by fitting the spin-wave frequencies to Eq. (2) with the anisotropy constants contained in Eq. (1) as free fitting parameters.

Figure 4 shows a set of four typical BLS spectra for a Co film thickness of 20 Å as a function of the in-plane angle φ_H, between the direction of the external magnetic field with respect to the [001] direction. In the center of each spectrum the dominating peak of elastically scattered light is seen. At

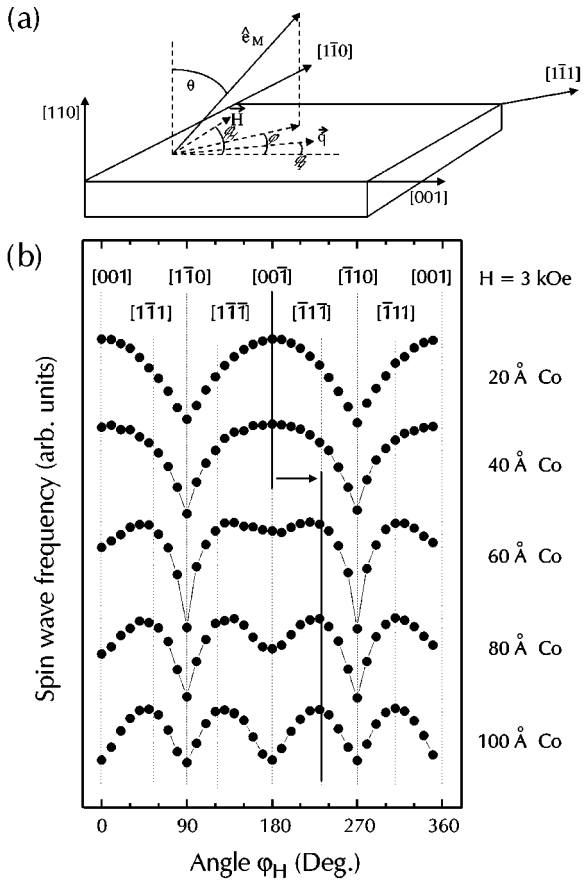

FIG. 5. (a) Experimental geometry. (b) Measured spin wave frequencies of 20–100 Å thick Co films on a Cu(110) single crystal covered by a 12 Å thick Cu overlayer as a function of the in-plane angle φ_H of the applied filed with respect to the [001] direction at an applied field of 3 kOe. The in-plane crystallographic directions are indicated by dashed lines. For clarity the spin-wave frequencies of each series are shifted (maximum variation: 30.0–38.6 GHz for d_{Co} = 20 Å; 20.0–25.1 Ghz for d_{Co}=100 Å).

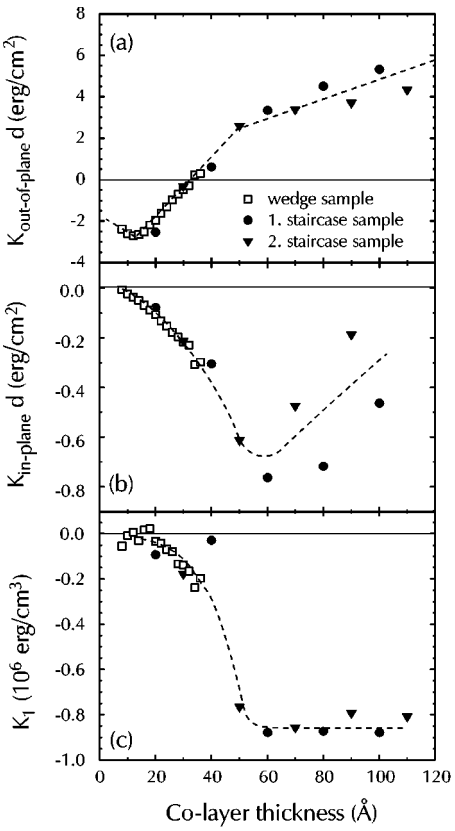

FIG. 6. (a) Effective out-of-plane anisotropy constant, $K_{\text{out-of-plane}}$, and (b) effective in-plane anisotropy constant, $K_{\text{in-plane}}$, multiplied with the Co film thickness d as a function of d. (c) magnetocrystalline anisotropy constant K_1 as a function of d. The dashed lines are guide lines to the eye. The three different symbols denote three different samples.

a frequency shift between 30 and 40 GHz the Damon-Eshbach spin wave[22] is clearly observed. For φ_H=0° ([001] direction) and φ_H=90° ([1$\bar{1}$0] direction) we find the highest and lowest spin-wave frequency values, respectively, indicating the easy and hard magnetization direction. By fitting the position of the spin-wave frequencies and plotting them as a function of the in-plane angle φ_H for different Co film thicknesses we obtain the data displayed in Fig. 5.

For d_{Co}=20 Å the spin-wave frequencies display a twofold behavior as a function of φ_H. The maxima of the spin-wave frequencies, indicating the easy magnetization directions, are found at φ_H = 0°, 180° and 360° (along ⟨001⟩ directions) clearly exhibiting a twofold in-plane symmetry with the easy axis of magnetization along the ⟨001⟩ axes. With increasing film thickness the pattern changes drastically. In the thickness regime between 40 and 60 Å the maxima of the spin wave frequencies and therefore the easy magnetization direction switch from the ⟨001⟩ axes toward the ⟨111⟩ axes. For d_{Co}=100 Å the maxima of the spin-wave frequencies found at the in-plane ⟨111⟩ axes are a clear signature for the presence of a dominating magnetocrystalline anisotropy (pseudo-fourfold symmetry). A detailed analysis, performed by fitting simultaneously the uniaxial anisotropy constants $K_{\text{in-plane}}$, $K_{\text{out-of-plane}}$ and the cubic bulk magnetocrystalline anisotropy constant K_1, yields as a function of film thickness the data displayed in Fig. 6.

Figure 6(a) shows the effective out-of-plane anisotropy constant, $K_{\text{out-of-plane}}$, multiplied by the Co film thickness d as a function of d. Such a plot yields the bulk anisotropy contributions as slopes and the interface anisotropy contributions as the (extrapolated) intercepts with the ordinate. At least two different thickness regimes can be identified. In the thickness regime between 13 and 50 Å we find a positive slope in $K_{\text{out-of-plane}} \cdot d$, indicating a large thickness-dependent magnetoelastic anisotropy contribution due to progressive strain relaxation. The mechanism of this anisotropy behavior is the anisotropic strain relaxation observed in the LEED and STM data (see Figs. 2 and 3). For $d_{\mathrm{Co}} >$ 50 Å we find a reduction in slope which we interpret as the onset of the complete elastic and isotropic relaxation of the film as expected for larger thicknesses. In this regime we find that the anisotropy remains constant and nonzero ($K_{\text{out-of-plane}} \cdot d$ scales with d). This finding points to a morphology-induced anisotropy contribution caused by, e.g., residual strains or a three-dimensional dislocation network which might persist to very large film thicknesses, or to a reduced demagnetization factor caused by the onset of columnar growth in this thickness regime [see Fig. 3(d)].

The structural information is paralleled by the observed effective in-plane anisotropy constant, $K_{\text{in-plane}} \cdot d$, which is

displayed as a function of d in Fig. 6(b). Assuming a magnetoelastic origin of the in-plane anisotropy, $K_{\text{in-plane}} \cdot d$ is proportional to the in-plane strain. The maximum absolute values of this anisotropy contribution are observed in the thickness regime between 50 and 70 Å. From the structural analysis we conclude that the elastic anisotropy in the in-plane strain has a maximum in this thickness regime as caused by the maximum anisotropy in the stripe shape of the Co islands [see Figs. 3(b) and 3(c)]. The two different staircase-type samples show a slightly different behavior for thicknesses larger than 50 Å [Fig. 6(b)]. Although both samples were prepared using the same recipe, the actual amount of strain relaxation seems to be very sensitive to minute details of the growth process.

In the thickness regime below 13 Å, the intercept for $d=0$ has a value of $2k_s=(-1.8\pm0.4)$ erg/cm^2. Since there are two Co/Cu interfaces this corresponds to a Néel interface anisotropy of (-0.9 ± 0.2) erg/cm^2 favoring in-plane magnetization. This confirms the orientational dependence of the interface anisotropy, which was reported to be (0.15 ± 0.04) erg/cm^2 for the (001) orientation[8,12] and (0.17 ± 0.05) erg/cm^2 for the (111) orientation.[14,30–32] We may associate the magnetoelastic anisotropy contribution K_S^{me} with K_S by the difference in the slopes between the regimes of pseudomorphic growth ($d_{\text{Co}}<13$ Å) and anisotropic strain relaxation due to misfit formation (13 Å $<d_{\text{Co}}<$ 50 Å). In the latter regime the obtained value of $K_S^{\text{me}}=(2.2\pm0.3)\times10^7$ erg/cm^3 is in close agreement with the value of $K_S^{\text{me}}=1.7\times10^7$ erg/cm^3 calculated using bulk magnetostriction constants.[33] Equivalently, we can identify the difference in intercept of the extrapolated linear fits of coherent [$2k_s=(-1.8\pm0.4)$ erg/cm^2] and (partially) incoherent growth [$2k_s=(-4.6\pm0.2)$ erg/cm^2] with a misfit interface anisotropy of (1.4 ± 0.3) erg/cm^2 as discussed in Refs. 18,19.

Figure 6(c) shows the magnetocrystalline anisotropy constant K_1 as a function of the film thickness d. For $d_{\text{Co}}>$ 50 Å a thickness independent value of $K_1=-(0.85\pm0.05)\times10^6$ erg/cm^3 is found which agrees with literature values for fcc Co.[2–4] For a Co film thickness below 50 Å we find a sudden breakdown of the magnetocrystalline anisotropy. This breakdown coincides with the maximum absolute value of the uniaxial in-plane anisotropy. This leads to the conclusion that the breakdown of the magnetocrystalline anisotropy is correlated with the in-plane anisotropy and therefore depends on the in-plane strain of the Co films.

To gain further insight, Co(110) films have been grown onto a 60 Å $Cu_{62}Ni_{38}$ buffer layer deposited onto a (110)-oriented Cu single-crystal substrate. Since the $Cu_{62}Ni_{38}$ buffer layer is relaxed the in-plane strain components are reduced by about a factor of 2 due to the smaller lattice mismatch of -1% between the CuNi buffer layer and the Co layer.

The misfit strain enters via tetragonal distortions the uniaxial anisotropy contributions. Hence, as expected, for the Co film grown on the CuNi buffer layer the transition thicknesses between the different anisotropy regimes are shifted with respect to the Co film grown directly onto the Cu(110) substrate. More surprisingly we find that the onset of the suppression of the magnetocrystalline anisotropy is shifted to larger thicknesses (Fig. 7): We find 50 Å for Co films on Cu(110), whereas we find the onset at about 100 Å for Co films on the CuNi buffer layer. A doubling of the critical thickness for reducing the strain by a factor of 2 is in good agreement with the usual model of the strain relaxation process.[18] We conclude that the misfit strain also enters the magnetocrystalline anisotropy.

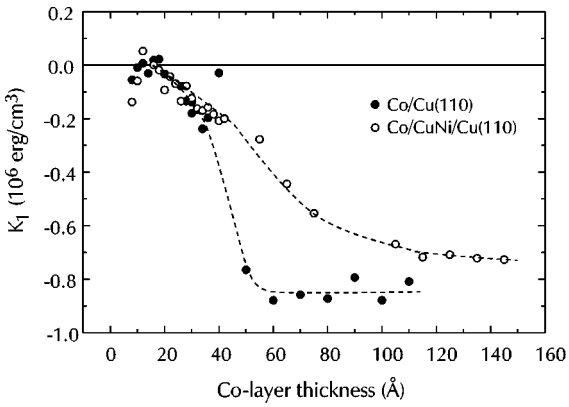

FIG. 7. Magnetocrystalline anisotropy constant K_1 as a function of the Co film thickness for Co films with (●) and without $Cu_{62}Ni_{38}$ buffer layer (○).

An important consequence is that the different anisotropy energy contributions are not independent from each other as presumed in Eq. (1). Since the microscopic origin of all contributing anisotropy terms is the electronic band structure and explicitly the spin-orbit coupling, one should also not expect this. As a consequence whenever the above described model is applied one has to think about its validity. Our experiments show clear evidence for this. In the following section we will discuss the phenomenon of the suppression of the magnetocrystalline anisotropy within symmetry reflections based on a crystal-field formalism, which explicitly takes into account tetragonal distortions.

V. SYMMETRY REFLECTIONS

The experimental data presented in the previous sections demonstrate that the presence of a uniaxial strain in the Co films strongly suppresses the cubic magnetocrystalline anisotropy. We now outline a model which provides new insight into the relationship between the second-order and fourth-order anisotropies.

The main problem of a suitable theoretical model for calculating magnetic anisotropies from first principles is the high-energy resolution required. In principle there are two different approaches—calculations based on the electronic band structure[34–40] and phenomenological models.[1,41,42] The Néel model[1] examines the magnetic anisotropy that is developed as a function of the angle made by the magnetization of a pair of sites and the line joining them. When this is summed over all the neighbors a cubic anisotropy is developed for a bulk crystal and surface anisotropy for those sites at the surface. The approach which is used here parallels the band-structure approach and recasts this into a form which is commonly used for magnetic insulators. This was developed because it is hard to do a real band theoretic calculation which has sufficient accuracy to reproduce the cubic anisot-

ropy reliably although there has been a recent advance in this respect.[43]

In a perturbation approach to a calculation of the anisotropy using a first-principles method one calculates the band states E_k^λ which are filled up by the correct number of electrons to define the Fermi level. The ground-state energy is found by adding up all the energies of the occupied states. In the presence of strains the Brillouin zone is distorted away from cubic. The spin-orbit coupling may now be considered as a perturbation, as it has the symmetry of the lattice it will cause admixtures only of states which have the same k value (but different values of λ). In second order it can give rise to a uniaxial anisotropy, and the cubic anisotropy first appears in fourth order. The new ground-state energy is found (by summing up the energies of the occupied states) for selected directions of magnetization and the magnetic anisotropy is found by subtraction. The approximate method which has been used here has inverted the order of k sum over the Brillouin zone and application of the perturbation produced by the spin-orbit coupling. The sum over the k states for a given band λ will give rise to a state which transforms like one of the irreducible representations of the crystalline point group. We work in the representations of the point group and takes the lattice symmetry fully into account. The wave functions relevant to our analysis are the $3d$ states, which are $x'y'$, $y'z'$, $x'z'$, $x'^2-y'^2$, and $3z'^2-r^2$ with x',y',z' the Cartesian coordinates of the electrons in the crystallographic reference frame and $r^2=x'^2+y'^2+z'^2$. The surface normal is along $z'=(x'+y')/\sqrt{2}$. We consider a Hamiltonian in terms of Steven's operators[44] in the form

$$H=A(l_{x'}^4+l_{y'}^4+l_{z'}^4)+X(l_{x'}+l_{y'})^2, \tag{3}$$

where A and X are the cubic and uniaxial energy parameters, respectively. From Eq. (3) it is apparent that we consider a uniaxial distortion of the unit cell along the growth direction (which is caused by strain), parametrized by the uniaxial energy parameter X, in addition to cubic symmetry, described by the cubic energy parameter A. We calculate anisotropies in the usual way by including the spin-orbit coupling as a perturbation.[45] Assuming that the exchange splitting is very large compared to the spin-orbit coupling we may write the perturbation for the magnetization along the axis ν as

$$E^{\mathrm{SO}}=\xi\vec{\ell}\cdot\vec{s}\approx\xi l_\nu/2. \tag{4}$$

The anisotropy energy is found by calculating the change in the ground-state energy for different directions ν, as a power series in the spin-orbit coupling constant ξ. Hence, we obtain expressions for the anisotropy energy to both second and fourth order in ξ.

The uniaxial energy parameter X is by definition proportional to the misfit strain ϵ. Chappert and Bruno[18] and also den Broeder *et al.*[46] argue that ϵ is inversely proportional to the film thickness and so we plot the anisotropies as functions of A/X which is therefore proportional to the film thickness. The experimental data and the calculated anisotropies are plotted in Fig. 8.

Figure 8 shows the magnetocrystalline anisotropy constant K_1 (a), the effective in-plane anisotropy constant $K_{\text{in-plane}}$ (b), and effective out-of-plane anisotropy constant $K_{\text{out-of-plane}}$ (c) of the experimental data (left panel) as a function of the Co film thickness and the calculation (right panel) as a function of the ratio of the cubic and uniaxial energy parameters A/X. For the model calculation the parameters A and ξ are chosen such that (i) K_1 approaches its experimental value for large thicknesses, and (ii) we obtain the correct value for $K_{\text{out-of-plane}}$ in the limit $X\gg A$. We have $A/\xi=8.8$ and $\xi=8$ meV/Co. Our value of ξ is approximately 10% of that used by Cinal *et al.*[37,38] Given the simplicity of our model in which effects of the spin-orbit coupling will be overestimated, we regard this as satisfactory.

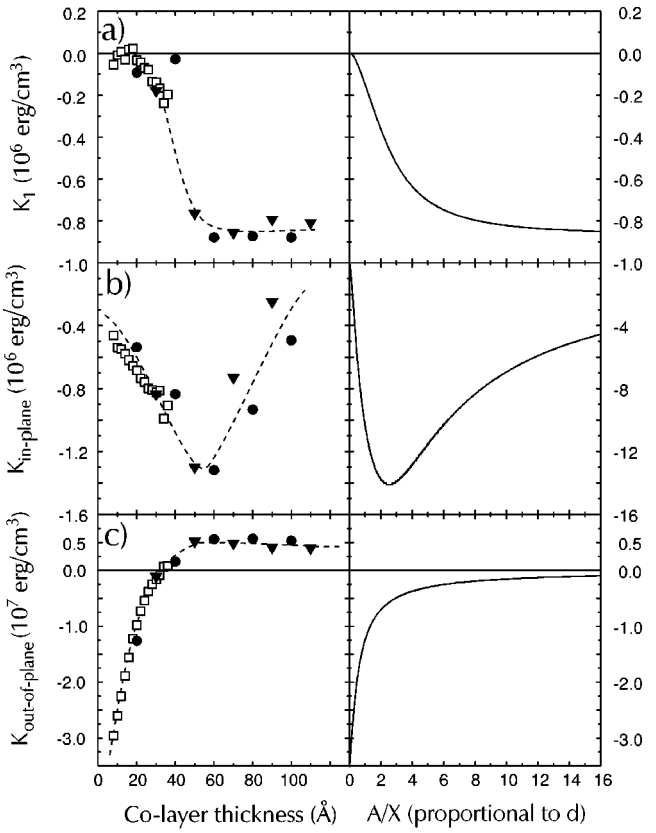

FIG. 8. Left panel: Experimental values (see Fig. 6): (a) magnetocrystalline anisotropy constant K_1; (b) effective in-plane anisotropy constant $K_{\text{in-plane}}$; and (c) effective out-of-plane anisotropy constant, $K_{\text{out-of-plane}}$; all plotted as a function of the Co film thickness, d. Right panel: (a) Calculated cubic anisotropy constant K_1; (b) second-order in-plane anisotropy constant, $K_{\text{in-plane}}$; and (c) second-order out-of-plane anisotropy constant $K_{\text{out-of-plane}}$, as a function of the ratio of the cubic and uniaxial energy parameters A/X, which is proportional to d.

Within our calculation the onset of the suppression of the magnetocrystalline anisotropy is correlated with the maximum absolute value of the uniaxial in-plane anisotropy constant [Fig. 8 (b)] and a notable change in the uniaxial out-of-plane anisotropy [Fig. 8 (c)]. This is in fact a good agreement with the experimental data. The physical origin can be explained as follows: The fourth-order anisotropy energy depends upon $\xi^4/(\text{excitation energy})^3$, where the relevant excitation energy is some combination of X and A: Hence for $X=0$, K_1 is proportional to ξ^4/A^3, but for $X\gg A$ we find K_1 is proportional to ξ^4/X^3. This qualitative behavior of the model is independent of the sign of A or X and hence of our

crystal-field ground state that we impose. However, in order for the cubic anisotropy to have the correct sign we take $A>0$. In this way we can understand that all anisotropy contributions change their behavior near $A/X\approx 1$. In this regime the transition from the uniaxial to the cubic symmetry-dominated regime takes place. For the magnitude of the uniaxial in-plane anisotropy constant $K_{\text{in-plane}}$, we find a discrepancy of one order of magnitude between experiment and theory. With the LEED and STM data in mind (Figs. 2 and 3) this is not surprising. The model described in this section assumes an isotropic strain relaxation, which is not fulfilled in the experiment. Since we found anisotropic strain relaxation, additional uniaxial in-plane strain components can occur giving rise to a modified uniaxial in-plane anisotropy contribution, which might account for the discrepancy between theory and experiment.

VI. CONCLUSION

We have determined all anisotropy contributions present in the epitaxial system Co/Cu(110). The structural origin of most of these anisotropy contributions was identified. We have identified the thickness regimes of pseudomorphic growth, anisotropic, and isotropic strain relaxation in the structure and the corresponding magnetic anisotropies of the Co films. A strong suppression of the magnetocrystalline anisotropy below a critical thickness of 50 Å was determined and was found to depend on the uniaxial growth-induced misfit strain. The origin was discussed within symmetry reflections. The transition from the uniaxial, strain-dominated thickness regime to a cubic, more bulklike behavior is shown experimentally in full agreement with model calculations. All anisotropy contributions change as a function of strain.

From our model calculations and the presented experimental evidence we conclude that a linear superposition of independent anisotropy terms in the free anisotropy energy, as it is often assumed to be valid, needs to be carefully tested for each system, in particular in the presence of higher-order anisotropy terms. This is not surprising taking into account that all anisotropy contributions originate from the same microscopic origin, namely the spin-orbit coupling.

ACKNOWLEDGMENTS

We thank U. May for his technical assistance. This work has been supported in part by the Deutsche Forschungsgemeinschaft through SFB 341. Support by the HCM programme of the European Community under Contract No. CHRX-CT93-0316 is gratefully acknowledged. D.J.R. acknowledges support from the EPSRC.

*Present address: IBM Research Division, Zurich Research Laboratory, CH-8803 Rüschlikon, Switzerland.

†Present address: Department of Physics, Eindhoven University of Technology, NL-5600 MB Eindhoven, The Netherlands.

[1] L. Néel, J. Phys. Radium **15**, 225 (1954).

[2] Data on rather thick fcc Co(110) films indicate the presence of a magnetocrystalline anisotropy contribution in addition to growth-induced uniaxial anisotropies. See C.-A. Chang, Appl. Phys. Lett. **58**, 1745 (1991).

[3] D. S. Rodbell, J. Phys. Soc. Jpn. **17**, 313 (1962).

[4] W. D. Doyle and P. J. Flanders, Proc. Phys. Soc. London **86**, 751 (1965).

[5] B. Hillebrands, A. Boufelfel, C. M. Falco, P. Baumgart, G. Güntherodt, E. Zirngiebl, and J. D. Thompson, J. Appl. Phys. **63**, 3880 (1988).

[6] B. Heinrich, J. F. Cochran, M. Kowalewski, J. Kirschner, Z. Celinski, A. S. Arrott, and K. Myrtle, Phys. Rev. B **44**, 9348 (1991).

[7] A. Berger, U. Linke, and H. P. Oepen, Phys. Rev. Lett. **68**, 839 (1992).

[8] P. Krams, F. Lauks, R. L. Stamps, B. Hillebrands, and G. Güntherodt, Phys. Rev. Lett. **69**, 3674 (1992).

[9] H. P. Oepen, C. M. Schneider, D. S. Chuang, C. A. Ballentine, and R. C. O'Handley, J. Appl. Phys. **73**, 6186 (1993).

[10] P. Krams, F. Lauks, R. L. Stamps, B. Hillebrands, G. Güntherodt, and H. P. Oepen, J. Magn. Magn. Mater. **121**, 483 (1993).

[11] H. P. Oepen, A. Berger, C. M. Schneider, T. Reul, and J. Kirschner, J. Magn. Magn. Mater. **121**, 490 (1993).

[12] M. Kowalewski, C. M. Schneider, and B. Heinrich, Phys. Rev. B **47**, 8748 (1993).

[13] P. Krams, B. Hillebrands, G. Güntherodt, and H. P. Oepen, Phys. Rev. B **49**, 3633 (1994).

[14] B. Hillebrands, P. Krams, J. Fassbender, C. Mathieu, G. Güntherodt, R. Jungblut, and M. T. Johnson, Acta Phys. Pol. A **85**, 179 (1994).

[15] B. Hillebrands, J. Fassbender, P. Krams, C. Mathieu, G. Güntherodt, and R. Jungblut, Il Vuoto, Scienza e Technologia **25**, 24 (1997).

[16] Limitations of this assumption are discussed in U. Gradmann, I. Korrecki, and G. Waller, Appl. Phys. A: Solids Surf. **39**, 110 (1986).

[17] C.-A. Chang, Appl. Phys. Lett. **58**, 1745 (1991).

[18] C. Chappert and P. Bruno, J. Appl. Phys. **64**, 5736 (1988).

[19] R. Jungblut, M. T. Johnson, J. aan de Stegge, A. Reinders, and F. J. A. den Broeder, J. Appl. Phys. **75**, 6424 (1994).

[20] G. Harp, R. F. C. Farrow, D. Weller, T. A. Rabedeau, and R. F. Marks, Phys. Rev. B **48**, 17 538 (1993).

[21] R. Mock, B. Hillebrands, and J. R. Sandercock, J. Phys. E **20**, 656 (1987).

[22] R. W. Damon and J. R. Eshbach, J. Phys. Chem. Solids **19**, 308 (1961).

[23] B. Hillebrands, Phys. Rev. B **41**, 530 (1990).

[24] R. L. Stamps and B. Hillebrands, Phys. Rev. B **44**, 12 417 (1991).

[25] A. K. Schmid and J. Kirschner, Ultramicroscopy **42-44**, 483 (1992).

[26] J. Fassbender, U. May, B. Schirmer, R. M. Jungblut, B. Hillebrands, and G. Güntherodt, Phys. Rev. Lett. **75**, 4476 (1995).

[27] J. de la Figuera, J. E. Prieto, C. Ocal, and R. Miranda, Phys. Rev. B **47**, 13 043 (1993).

[28] J. Camarero, L. Spendeler, G. Schmidt, K. Heinz, J. J. de Miguel, and R. Miranda, Phys. Rev. Lett. **73**, 2448 (1994).

[29] A. Rabe, N. Memmel, A. Steltenpohl, and Th. Fauster, Phys. Rev. Lett. **73**, 2728 (1994).

[30] M. T. Johnson, J. J. de Vries, N. W. E. McGee, J. aan de Stegge, and F. J. A. den Broeder, Phys. Rev. Lett. **69**, 3575 (1992).

[31] J. Kohlhepp, H. J. Elmers, and U. Gradmann, J. Magn. Magn. Mater. **121**, 487 (1993).

[32] M. Sakurai and T. Shinjo, J. Phys. Soc. Jpn. **62**, 1853 (1993).

[33] B. Hillebrands and J. R. Dutcher, Phys. Rev. B **47**, 6126 (1993).

[34] G. H. O. Daalderop, P. J. Kelly, and M. F. H. Schuurmans, Phys. Rev. B **41**, 11 919 (1990).
[35] G. Y. Guo, W. M. Temmerman, and H. Ebert, Physica B **172**, 61 (1991).
[36] G. H. O. Daalderop, P. J. Kelly, and F. J. A. den Broeder, Phys. Rev. Lett. **68**, 682 (1992).
[37] M. Cinal, D. M. Edwards, and J. Mathon, Phys. Rev. B **50**, 3754 (1994).
[38] M. Cinal, D. M. Edwards, and J. Mathon, J. Magn. Magn. Mater. **140-144**, 681 (1995).
[39] R. Lorenz and J. Hafner, J. Phys.: Condens. Matter **7**, L253 (1995).
[40] B. Ujfalussy, L. Szunyogh, P. Bruno, and P. Weinberger, Phys. Rev. Lett. **77**, 1805 (1996).
[41] D. S. Wang, R. Q. Wu, and A. J. Freeman, J. Magn. Magn. Mater. **129**, 237 (1994).
[42] B. Hillebrands, J. Fassbender, R. Jungblut, G. Güntherodt, D. J. Roberts, and G. A. Gehring, Phys. Rev. B **53**, 10 548 (1996).
[43] D. J. Roberts, G. Y. Guo, and G. A. Gehring (unpublished).
[44] K. W. H. Stevens and C. A. Bates, in *Magnetic Oxides*, edited by D. J. Craik (Wiley, New York, 1975).
[45] D. J. Craik, *Magnetism, Principles and Applications* (Wiley, Chichester, 1995).
[46] F. J. A. den Broeder, W. Hoving, and P. J. H. Bloemen, J. Magn. Magn. Mater. **93**, 562 (1991).